Cell Reports
Report

Mutations in the β-Tubulin Gene *TUBB5* Cause Microcephaly with Structural Brain Abnormalities

Martin Breuss,[1,11] Julian Ik-Tsen Heng,[2,11] Karine Poirier,[3] Guoling Tian,[4] Xavier Hubert Jaglin,[3] Zhengdong Qu,[2] Andreas Braun,[1] Thomas Gstrein,[1] Linh Ngo,[2] Matilda Haas,[2] Nadia Bahi-Buisson,[3] Marie-Laure Moutard,[5] Sandrine Passemard,[6,7] Alain Verloes,[6,7] Pierre Gressens,[6] Yunli Xie,[8] Kathryn J.H. Robson,[9] Deepa Selvi Rani,[10] Kumarasamy Thangaraj,[10] Tim Clausen,[1] Jamel Chelly,[3] Nicholas Justin Cowan,[4] and David Anthony Keays[1,*]
[1]Institute of Molecular Pathology, Dr Bohr-Gasse, Vienna 1030, Austria
[2]Australian Regenerative Medicine Institute, Monash University, Clayton, Victoria 3800, Australia
[3]Institut Cochin; INSERM Unité 1016; CNRS UMR 8104; Université Paris Descartes, Sorbonne Paris Cité Paris, France
[4]Department of Biochemistry and Molecular Pharmacology, New York University Medical Center, New York, NY 10016, USA
[5]Service de Neurologie Pediatrique, AP-HP, Hopital Trousseau, Paris, 75571, France
[6]INSERM UMR-676, Robert Debré Hospital, Paris, 75019, France
[7]Paris Diderot University, Department of Génétics, Robert Debré Hospital, Paris, France
[8]Institute of Molecular Biotechnology, Dr Bohr-Gasse 3, Vienna, Austria
[9]MRC Weatherall Institute of Molecular Medicine, University of Oxford, John Radcliffe Hospital, Oxford, OX3 9DS, United Kingdom
[10]Centre for Cellular and Molecular Biology, Habsiguda, Uppal Rd, Hyderabad 500 007, India
[11]These authors contributed equally to this work
*Correspondence: keays@imp.ac.at
http://dx.doi.org/10.1016/j.celrep.2012.11.017

SUMMARY

The formation of the mammalian cortex requires the generation, migration, and differentiation of neurons. The vital role that the microtubule cytoskeleton plays in these cellular processes is reflected by the discovery that mutations in various tubulin isotypes cause different neurodevelopmental diseases, including lissencephaly (*TUBA1A*), polymicrogyria (*TUBA1A*, *TUBB2B*, *TUBB3*), and an ocular motility disorder (*TUBB3*). Here, we show that *Tubb5* is expressed in neurogenic progenitors in the mouse and that its depletion in vivo perturbs the cell cycle of progenitors and alters the position of migrating neurons. We report the occurrence of three microcephalic patients with structural brain abnormalities harboring de novo mutations in *TUBB5* (M299V, V353I, and E401K). These mutant proteins, which affect the chaperone-dependent assembly of tubulin heterodimers in different ways, disrupt neurogenic division and/or migration in vivo. Our results provide insight into the functional repertoire of the tubulin gene family, specifically implicating *TUBB5* in embryonic neurogenesis and microcephaly.

INTRODUCTION

The formation of the mammalian cortex, a complex multilayered structure, requires the birth of neurons in the ventricular and subventricular zones followed by phases of bipolar and multipolar migration before newly born neurons arrive at their final destination in the cortical plate (Feng and Walsh, 2001). This sophisticated cellular journey relies on a myriad of intracellular and intercellular signaling factors that converge on the cytoskeleton (Ayala et al., 2007). The importance of the microtubule cytoskeleton in the sequential steps involved in migration and differentiation is reflected in the finding that mutations in various tubulin genes cause a range of structural brain abnormalities. Mutations in the α-tubulin subunit *TUBA1A* have been shown to result in lissencephaly (Keays et al., 2007); mutations in the β-tubulin subunit *TUBB2B* cause asymmetric polymicrogyria (Jaglin et al., 2009); and it has been shown that mutations in *TUBB3* cause an ocular motility disorder (Tischfield et al., 2010), as well as a broad range of cortical abnormalities (Poirier et al., 2010). Most recently, the tubulin genes *TUBA1A* and *TUBB2B* have also been implicated in autism spectrum disorders (Neale et al., 2012; Pinto et al., 2010). Together, these studies have implicated specific tubulin isotypes in postmitotic cellular events, but those isotypes that mediate the generation of neurons, a process that requires the assembly of microtubules into a highly organized mitotic spindle, remain unknown (Ohnuma and Harris, 2003). Here, we set out to identify those tubulin genes required for cortical neurogenesis. We report that the β-tubulin gene *TUBB5* is highly expressed in the developing cortex and that mutations in this gene cause microcephaly, with a range of structural brain abnormalities that include dysmorphic basal ganglia, dysgenesis of the corpus callosum, brainstem hypoplasia, and focal polymicrogyria.

RESULTS AND DISCUSSION

Tubb5 Is Expressed at High Levels in the Developing Brain

We surveyed the expression of all known β-tubulin genes in the developing mouse (E10.5, E12.5, E14.5, E16.5, P0) and

human (gestational week [GW] 13, GW22) cortex by quantitative real-time PCR (Braun et al., 2010). We observed consistently high expression levels of *Tubb2b*, *Tubb3,* and *Tubb5*, with *Tubb5* the highest expressed isotype in the embryonic mouse brain (Figures 1A and 1B). We investigated the spatial expression of *Tubb5* by in situ hybridization at embryonic day (E) 12.5, E14.5, and E16.5 (Figures 1C–1H). This revealed robust expression throughout the developing cortex, particularly in the subventricular zone (SVZ) at E14.5, which was absent in sense controls (Figures S1A–S1C). Because there are no validated antibodies that are specific for *Tubb5,* we created a transgenic mouse line that drives enhanced green fluorescent protein (EGFP) from the endogenous *Tubb5* promoter to determine which cell types express *Tubb5* (Figures S1D–S1Q). This mouse recapitulated our in situ hybridization results and demonstrated that *Tubb5* is expressed in radial glial cells (Pax6 positive), intermediate progenitors (Tbr2 positive), migrating neurons (Dcx positive), and postmitotic neurons (Tuj positive; Figures 1I–1X).

Depletion of *Tubb5* Perturbs the Progenitor Cell Cycle and the Migration of Neurons

We investigated the effect of *Tubb5* depletion on cortical development in mice by employing a small hairpin RNA (shRNA) that targets its 3′UTR. Following validation of this shRNA in Neuro-2a cells (Figure S2A), we electroporated it into progenitor cells of the ventricular zone (VZ) at E14.5, together with a GFP expressing vector (Figure 2A). Quantification of the fraction of GFP-positive cells that coexpress pH3 (mitotic index) after 36 hr of knockdown revealed an increase in the percentage of these mitotic cells in the VZ/SVZ when *Tubb5* was depleted ($n = 6$; $p < 0.001$). This effect could be rescued by codelivering a *Tubb5* expression construct that lacked the shRNA targeting sequence (Figures 2B–2D; Figures S2D and S2E; Table S2) and replicated when employing an alternative shRNA (data not shown). Because mutations in *Tuba1a* have been shown to induce apoptosis, we studied cell survival by staining for cleaved caspase-3 at E16, following electroporation at E14.5 (Edwards et al., 2011). This revealed no statistically significant difference between conditions, but we cannot exclude the possibility of increased apoptosis following long-term depletion of *Tubb5* (Figures S2F–S2O). Next, we investigated the effect of *Tubb5* depletion on neuronal migration by electroporating our shRNA at E14.5 and harvesting embryos 72 hr later (migration index). In comparison to controls, we observed a significant decrease in the percentage of GFP-labeled cells in the cortical plate (CP) when *Tubb5* was depleted, concomitant with an accumulation of cells within the VZ and intermediate zone (IZ) ($n \geq 5$; VZ: $p < 0.05$; IZ: $p < 0.05$; CP: $p < 0.01$; Figures 2E–2G; Figures S2B and S2C; Table S2). To assess whether *Tubb5* depletion affects the final positioning of neurons, we harvested brains at postnatal day (P) 17, following electroporation at E14.5. Quantification of the percentage of GFP positive cells in the six layers of the P17 cortex showed that *Tubb5* knockdown results in a long-term positioning defect ($n = 4$; layer VI: $p < 0.05$; layers II–IV: $p < 0.01$) (Figure 2H). We conclude that *Tubb5* depletion perturbs the neurogenic cell cycle and alters the positioning of migrating neurons.

Mutations in *TUBB5* Cause Microcephaly in Humans

On the basis of these results, we surmised that mutations in *TUBB5* might cause neurodevelopmental disease in humans. We therefore screened a panel of patients with a range of brain malformations, resulting in the identification of three unrelated microcephalic individuals harboring de novo mutations in *TUBB5* (M299V, V353I, and E401K) (Figures S3A–S3C). Each individual presented with microcephaly (with an orbitofrontal cortex [OFC] ranging from −2.5 SD to −4 SD), dysmorphic basal ganglia, corpus callosum abnormalities, and cognitive impairment with motor and language delay (Table 1; Figures 3A–3F; Figures S3E and S3F). Two of the patients (M299V and V353I) shared unusual white matter streaks with a radial orientation through the lenticular nucleus, as well as brainstem hypoplasia (Figures 3A–3F). The child harboring the V353I mutation originates from a family with a history of microcephaly (without mental retardation), raising the prospect that another genetic factor contributes to his disease. Sequencing of known microcephaly genes (*MCPH1*, *CD5KRAP2*, *WDR62*, *ASPM*) and the known disease causing tubulins (*TUBA1A*, *TUBB2B,* and *TUBB3*) did not identify any pathogenic variants in the patients described. A search of publicly available genomic databases showed that the M229V, V353I, and E401K mutations are not present in the general population. Moreover, screening of ethnically relevant controls (French/Caucasian, 238; Vietnamese, 115; Indian subcontinent, 252) failed to identify these variants. Homology analysis showed that these residues are highly conserved in all human β-tubulins and related tubulin isotypes from yeast to humans (Figure S3D).

Functional Analysis of Disease-Causing Mutations

We mapped the location of the affected residues onto the known structure of the α/β heterodimer (Figures 3G–3J). M299 lies in a loop following helix 9, with its side chain protruding into a deep hydrophobic pocket. V353 lies on the intradimer interface, whereas E401, which precedes helix 12, lies on the surface of the interdimer interface. This residue is in close proximity to a loop (αα98–104) that is critical for nucleotide binding (Löwe et al., 2001) and that may be reoriented by substitution with a lysine residue. All three mutations have the potential to compromise either the complex chaperone-dependent reactions that are essential for tubulin heterodimer assembly or the dynamic behavior of microtubules (Tian et al., 2010). To address these issues, we monitored the expression and folding of the mutant proteins kinetically in rabbit reticulocyte lysate. Analysis of the products under denaturing conditions showed that the translation efficiency of all three mutants was similar to the wild-type control (Figure 3K). However, analysis of the same reaction products under native conditions revealed quantitative and qualitative differences (Figure 3L). The wild-type protein and V353I and M299V mutants produced the expected folding intermediates (CCT/β, TBCD/β, PFD/β, and TBCA/β) (Cowan and Lewis, 2001) before generating α/β heterodimers when chased with native bovine tubulin, but with a notable reduction in yield for the M299V mutation. In the case of the E401K mutation, the assembly pathway was arrested, with a conspicuous retention of the mutant polypeptide complexed with prefoldin (PFD) and the cytosolic chaperonin (CCT), and a dearth of native

Cell PRESS
Open ACCESS

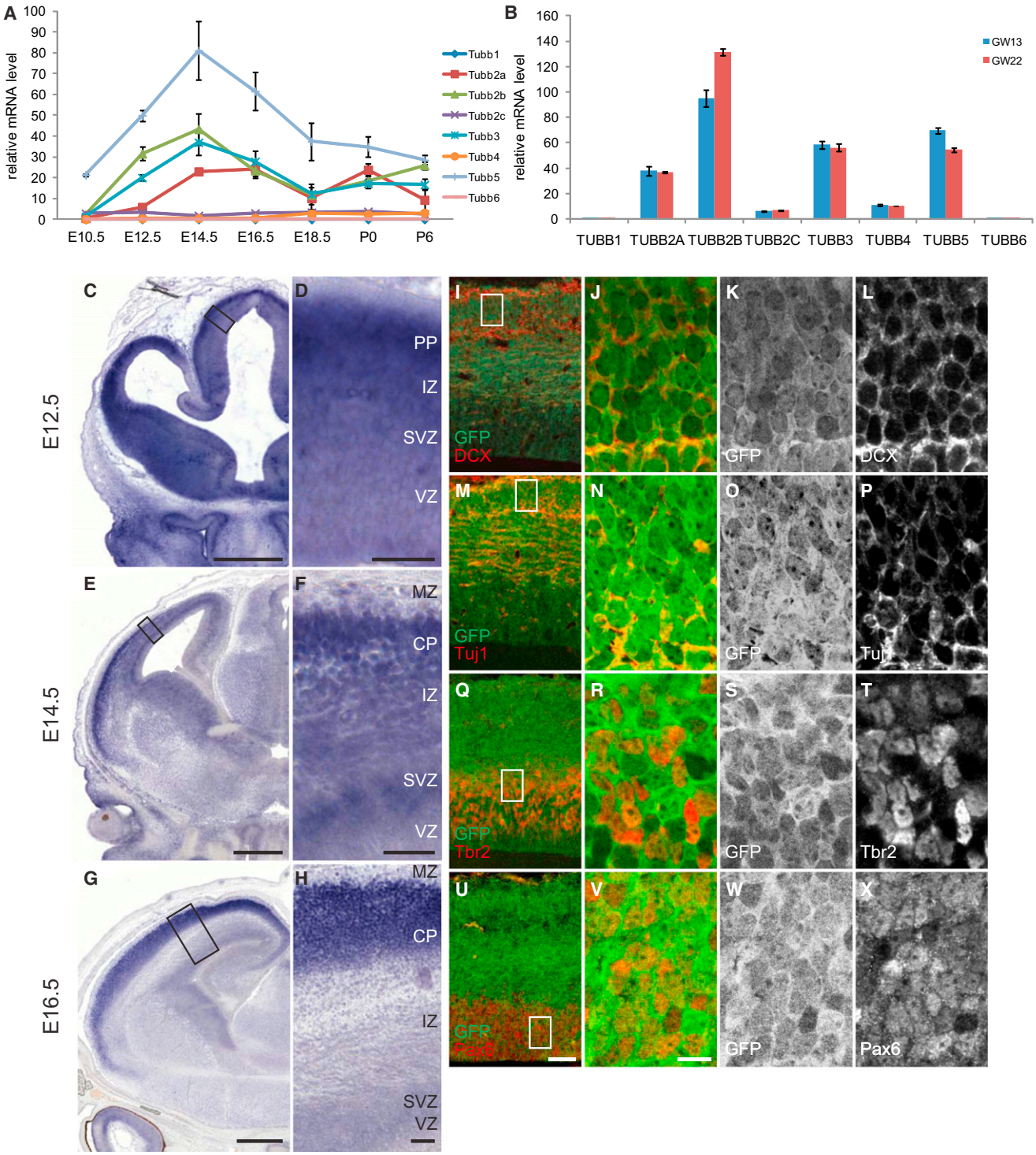

Figure 1. *Tubb5* Is Highly Expressed in the Developing Mouse and Human Brain

(A) Relative expression levels of β-tubulin genes in the developing mouse brain determined by quantitative real-time PCR at E10.5, E12.5, E14.5, E16.5, and E18.5 and postnatal days zero (P0) and six (P6) (n = 3). Note the early onset and consistently high expression of *Tubb5*.

(B) Relative expression levels of all the human β-tubulin genes in the developing brain at GW13 and GW22.

(C–H) In situ hybridization results obtained with an antisense probe specific for *Tubb5* at E12.5 (C and D), E14.5 (E and F), and E16.5 (G and H). (D), (F), and (H) show higher magnifications of (C), (E), and (G), respectively. *Tubb5* is detected throughout the developing cortex with strong expression in the preplate at E12.5, and in the SVZ at E14.5.

(legend continued on next page)

α/β heterodimers. We also examined the capacity of the TUBB5 mutants to incorporate into the microtubule network in Neuro-2a cells (Figures 3M–3X). Whereas the wild-type M299V and V353I proteins coassembled into interphase microtubules, we found that the E401K mutant protein failed to do so and was diffusely distributed throughout the cytoplasm. We conclude that the V353I and M299V mutations do not affect the ability of the mutant polypeptides to assemble into heterodimers and incorporate into microtubules, although the yield in the case of M299V may be compromised. In contrast, the E401K mutation results in a severe ablation of TUBB5 function, as it results in a massive failure of chaperone-mediated heterodimer assembly with a consequent inability of the mutant protein to incorporate into microtubules.

Effects of Human Mutations on Murine Neuronal Development

To examine the effect of these mutations in vivo, we used in utero electroporation to overexpress the mutant forms of *Tubb5* in the developing mouse brain. While overexpression of wild-type *Tubb5* had no effect on the mitotic index ($n = 5$; $p > 0.5$), we found a large increase in the percentage of GFP/pH3-colabeled cells in the VZ and SVZ when expressing the E401K and V353I mutants, similar to our *Tubb5* depletion experiments ($n = 5$; $p < 0.001$ for both mutants; Figures 4A, 4D, and 4E). Electroporation of the M299V expression construct also resulted in a modest increase in the mitotic index within the cortical germinal zone (VZ + SVZ), although this increase was not statistically significant ($n = 5$; $p > 0.05$; Figures 4A and 4C). We also examined the migratory index following expression of the *Tubb5* mutants. In comparison to controls, we found that expression of all three mutants resulted in a significant increase in the percentage of GFP-positive cells in the IZ and a corresponding decrease in the CP that was most severe in the case of the V353I mutant ($n = 5$; M299V: IZ: $p < 0.001$; CP: $p < 0.01$; V353I: VZ: $p < 0.01$; IZ: $p < 0.001$; CP: $p < 0.001$; E401K: IZ: $p < 0.001$; CP: $p < 0.01$; Figures 4B and 4G–4I). These changes were not observed upon overexpression of wild-type *Tubb5* alone ($n = 5$; $p > 0.05$; Figure 4F). Analysis of neurons at P17 following the overexpression of *Tubb5* mutants revealed aberrant clusters of ectopic cells in deep layers of the cortex (Figure S4). Quantification showed that in comparison to controls, this results in fewer cells in superficial layers of the cortex ($n \geq 2$; M299V: II–IV: $p < 0.05$; E401K: II–IV: $p < 0.001$) and an accumulation of GFP-positive cells in the deeper layers (E401K: $n = 3$; VI: $p < 0.01$), but this was not significant in the case of the V353I mutation ($n = 3$; VI: $p > 0.05$). This result demonstrates that the migratory defects described above have a long-term effect on neuronal position, and consequently on the structural architecture of the brain. Together, these data support our conclusion that the mutations are pathogenic, with an effect on both the generation and subsequent migration of neurons.

The three mutations we identified (M299V, V353I, and E401K) are likely to act by different molecular mechanisms (Walsh and Engle, 2010). The impairment in heterodimer assembly observed in the case of the E401K and M299V mutations suggests that they act by loss-of-function; however, the marked phenotype that results from heterologous expression of all mutants in vivo raises the prospect of a dominant-negative effect. It is conceivable that kinetically trapped E401K and M299V polypeptides have a deleterious effect on the entire chaperone-mediated tubulin folding and assembly pathway, while the V353I mutation may alter the dynamic properties of microtubules or compromise the binding of one or more essential microtubule associated proteins (Kumar et al., 2010; Tischfield et al., 2010; Walsh and Engle, 2010). The underlying cellular pathology is likely to be equally as complex. We have shown that both knockdown of Tubb5 and overexpression of Tubb5 mutants result in a paradoxical increase in pH3 reactivity. There are a number of explanations for this unexpected result, which implies an increase in mitotic output. First, it is conceivable that there is an elongation of M-phase, which delays progression of the cell cycle and the generation of neurons (Lizarraga et al., 2010). Second, it is possible that hyperproliferating apical progenitors result in fewer intermediate progenitors, and consequently an overall reduction in postmitotic neurons (Kim et al., 2009). Third, M-phase arrest may, at a later point in time, result in increased apoptosis, accounting for the incongruity between our in vivo pH3 results and the human phenotype. Further studies focused on the timing and output of the cell cycle will be necessary to establish which of the aforementioned mechanisms are responsible.

It is apparent from this study that patients with mutations in *TUBB5* share structural brain abnormalities in common with the previously described tubulinopathies (*TUBA1A*, *TUBB2B*, *TUBB3*), including dysmorphic basal ganglia, abnormalities of the corpus callosum, and brainstem phenotypes (Tischfield et al., 2011). The distinguishing feature of *TUBB5*-associated disease is microcephaly, which we attribute to the high level of *TUBB5* expression in neuronal progenitors. This contrasts with *TUBA1A*, *TUBB2B,* and *TUBB3,* all of which are largely restricted in their expression to postmitotic neurons in the developing brain (Gloster et al., 1999; Jaglin et al., 2009; Liu et al., 2007). *TUBB5* may have a specific function in mitotically active cells, or alternatively make a critical contribution to the supply of tubulin heterodimers. In either event, our work provides insight into the functional repertoire of the tubulin gene family, specifically implicating *TUBB5* in embryonic neurogenesis and microcephaly.

EXPERIMENTAL PROCEDURES

Animals

Animals were maintained within the animal research laboratories of the Institute of Molecular Pathology and Monash University on a 12:12 light:dark

(I–X) Antibody staining for Dcx (I–L), Tuj (M-P), Tbr2 (Q–T), and Pax6 (U–X) performed on coronal sections of the Tg (Tubb5-EGFP) mouse line at E14.5. Grey scale images of (J), (N), (R), and (V) are shown in (K) and (L), (O) and (P), (S) and (T), and (W) and (X). All markers were found to colocalize with or in GFP-positive cells.

Scale bars show 500 μm in (C), (E), and (G); 50 μm in (D), (F), and (H); 50 μm in (U); and 10 μm in (V). Error bars in (A) and (B) show SEM. See also Figure S1.

Cell PRESS
Open ACCESS

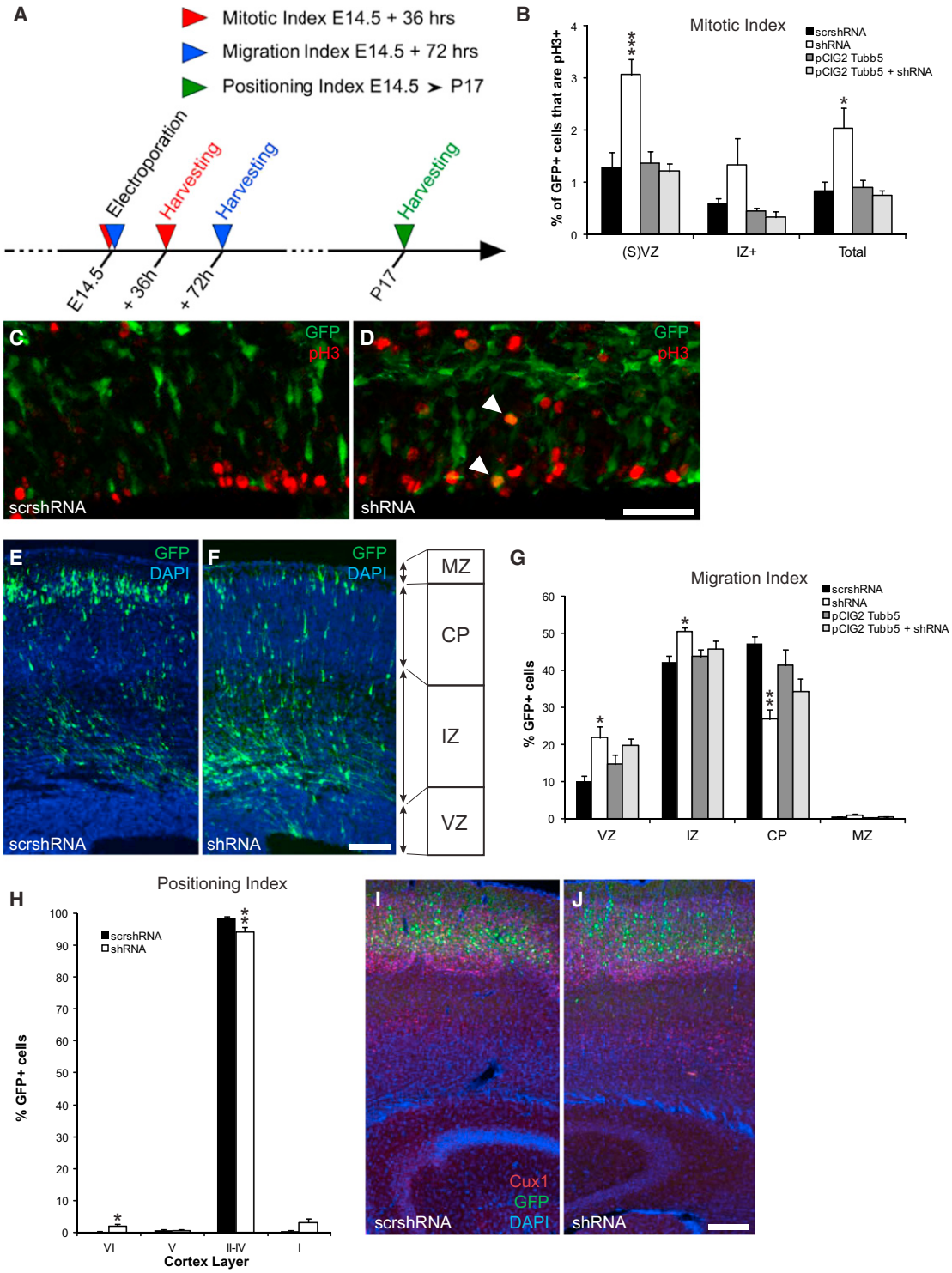

Figure 2. *Tubb5* Depletion Perturbs Progenitor Mitosis and Alters the Positioning of Postmitotic Neurons

(A) Schematic illustrating the three different in utero electroporation experiments. After electroporation at E14.5, embryos were harvested 36 hr later to assess the mitotic index, harvested 72 hr later to assess the migration index, or harvested at P17 to assess the positioning index.

(B) Quantitation of the mitotic index, showing the relative proportion of GFP positive cells that are also pH3 positive in the VZ and SVZ, IZ, and across all zones (Total) for the following conditions: scrambled shRNA (scrshRNA); shRNA targeting *Tubb5* (shRNA); overexpression of *Tubb5* (pCIG2 *Tubb5*); and the rescue experiment (pCIG2-*Tubb5* + shRNA). Note that *Tubb5* depletion results in a significant increase in the mitotic index in comparison to the scrambled control, overexpression, and rescue experiments ($n \geq 5$; VZ and SVZ: $p < 0.001$; Total: $p < 0.05$).

(legend continued on next page)

Table 1. Summary of Clinical, Neurological, Biochemical, Cellular and In Vivo Data Associated with *TUBB5* Mutations

	M299V	*V353I*	*E401K*
Ethnicity/Origin	Caucasian	Sri Lanka	Vietnam/Caucasian
Sex	Male	Male	Female
Age at last evaluation	2 years 6 months	4 years 10 months	2 years 8 months
OFC at birth	32 cm (−3 SD)	31 cm (−3 SD)	28.5 cm (−4 SD)
OFC at last evaluation	−2.5 SD	46.5 cm (−4 SD)	42 cm (−4 SD)
Cortical dysgenesis	Focal polymicrogyria, localized band heterotopia	None apparent	None apparent at 4 months
Basal ganglia	Dysmorphic White matter streaks	Dysmorphic White matter streaks	Dysmorphic
Cerebellum	Hypoplastic and dysplastic cerebellar vermis	Possible white matter abnormalities.	Large 4th ventricle
Corpus callosum	Partial agenesis	Thin and short but complete	Partial posterior agenesis
Cognitive abilities	Severe MR	MR (global DQ:48)	Mild developmental delay
Verbal abilities	Severe language delay	Limited language Speech delay.	Delayed
Motor abilities	Severe motor delay, ataxia	Motor delay. Walked at 21 months.	Motor delay. Walked at 25 months
Other	Retina dysplasia and micro-ophthalmia	None apparent.	Prenatal diagnosis of cardiopathy
Family history	None	Mother's OFC is −4 SD Brother's OFC is −2 SD Sister's OFC is −1 SD	None
Heterodimer folding	Slightly impaired	Not affected	Severely impaired
Microtubule lattice incorporation	Not affected	Not affected	No incorporation
Mitotic index	n.s.	Significantly increased	Significantly increased
Migration index	Significantly decreased	Significantly decreased	Significantly decreased
Positioning index	Affected	n.s.	Affected
Ectopic clusters at P17	Yes	Yes	Yes

OFC, orbitofrontal cortex; MR, mental retardation; DQ, development quotient; n.s., nonsignificant.

cycle with food available ad libitum. All procedures were performed in accordance with existing animal licenses and guidelines (M58-006093-2011-13 B).

Generation of Tg(Tubb5-EGFP) Mice

The Red/ET system (*K001*, Gene Bridges) was employed to replace the endogenous *Tubb5* (*RP24-330C1*) with EGFP. Following generation of the construct, we proceeded with pronuclear injection and PCR screening to confirm germline transmission before immunostaining.

In Situ Hybridization

C57/BL6 embryos were harvested, postfixed in 4% paraformaldehyde (PFA), dehydrated in a pressure- and temperature-controlled environment, embedded in paraffin, and sectioned (14 μm). We then proceeded with in situ hybridization as previously described (Braun et al., 2010).

Real-Time Quantitative PCR

Embryonic, postnatal, and adult tissues (C57/BL6) were dissected and snap frozen before mRNA extraction and reverse transcription. Quantitative

(C and D) Representative images for the mitotic index experiment. Arrowheads highlight colocalization of GFP-expressing cells (green) with pH3 staining (red). (E and F) Representative images showing the migration assessment following *Tubb5* depletion. Note the conspicuous reduction in the proportion of GFP-positive cells reaching the CP.

(G) Quantification of the percentage of GFP-positive cells in the VZ, IZ, CP, and marginal zone (MZ) for the migration index following treatment with a scrshRNA; an shRNA targeting *Tubb5* (shRNA); a *Tubb5* expression construct (pCIG2 *Tubb5*); and the rescue experiment (shRNA + pCIG2 *Tubb5*). *Tubb5* depletion results in a moderate but significant increase in the percentage of GFP-positive cells located in the VZ and IZ and a decrease in the percentage of GFP-positive cells in the CP ($n \geq 5$, VZ: $p < 0.05$; IZ: $p < 0.05$; CP: $p < 0.01$). This phenotype was partially rescued by coexpression of a *Tubb5* isotype lacking the shRNA targeting sequence (pCIG2 *Tubb5* + shRNA). Note that overexpression of *Tubb5* by itself has no effect on migration (pCIG2 *Tubb5*).

(H) Quantification of the percentage of GFP-positive cells in the six layers of the P17 cortex following treatment with an scrshRNA and a shRNA targeting *Tubb5*. *Tubb5* depletion results in a significant increase in the percentage of neurons in layer VI ($n = 4$; $p < 0.05$), with a concomitant decrease in layers II–IV ($n = 4$; $p < 0.01$).

(I and J) Representative images for the positioning index in (H). The red channel shows Cux1 staining in layers II–IV.

Scale bars show 50 μm in (D), 100 μm in (F), and 200 μm in (J). Error bars in (B), (G), and (H) show mean ± SEM.*$p < 0.05$, **$p < 0.01$, ***$p < 0.001$. MZ, marginal zone; scrshRNA , scrambled shRNA. See also Figure S2.

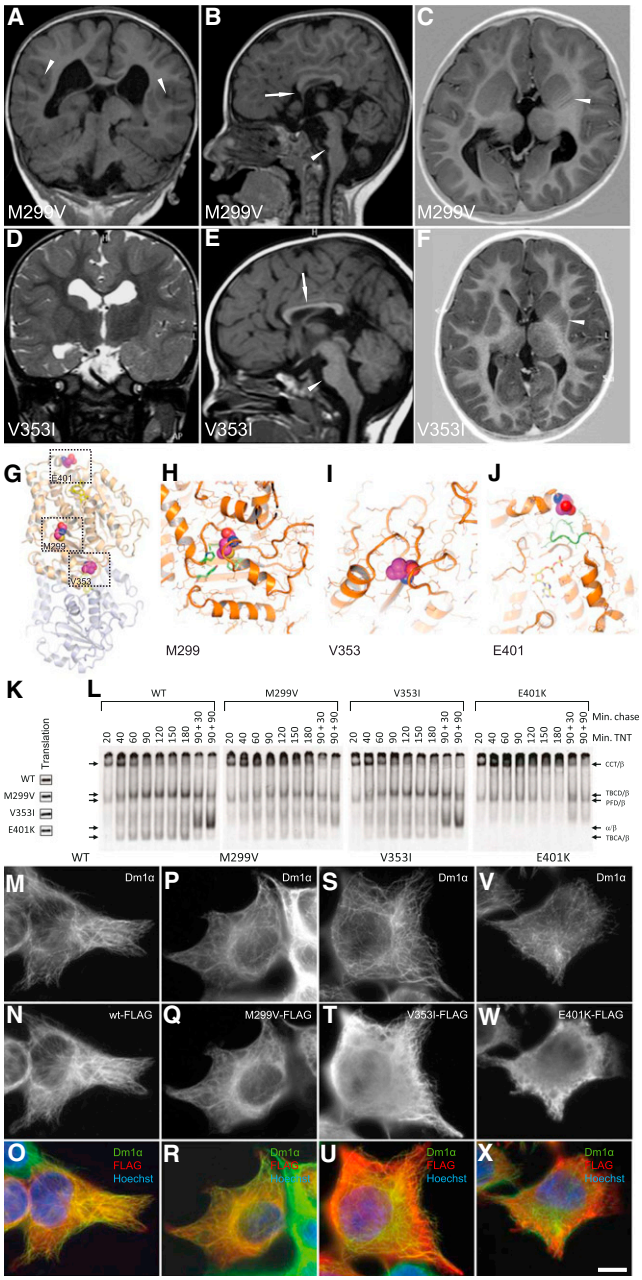

Figure 3. Mutations in *TUBB5* Cause Microcephaly and Affect the Generation of Tubulin Heterodimers in Different Ways

(A–F) Coronal (A and D), sagittal (B and E), and horizontal (C and F) MRIs of two patients with *TUBB5*-associated microcephaly (M299V and V353I). (A–C) The patient with the M299V mutation has microcephaly (OFC of −2.5 SD), focal polymicrogyria (shown with arrowheads in A), severe brainstem hypoplasia (shown with an arrowhead in B), partial agenesis of the corpus callosum (shown with an arrow in B), and dysmorphic basal ganglia with streaks of white matter (highlighted with an arrowhead in C). (D–F) The patient with the V353I mutation has microcephaly (OFC of −4.0 SD), a hypoplastic corpus callosum (shown with an arrow in E), and a dysmorphic basal ganglia with streaks of white matter running through the lenticular nucleus (shown with an arrowhead in F).

(G) Structural representation of a tubulin heterodimer highlighting the positions of the mutated residues. The M299 residue is centrally located and is associated with a deep hydrophobic pocket. V353 lies on the intradimer interface, in contrast to E401, which is located at the interdimer interface.

(H–J) Higher-resolution images showing the mutated residues within the three-dimensional structure of the tubulin heterodimer. (H) The M299 side chain is surrounded by hydrophobic residues (M267, P305, Y310, F367, shown in green) that could be disrupted by replacement with valine. (J) E401 lies in proximity to a loop (98–104, shown in green) that is critical for the binding of GTP (shown in yellow).

(K) Denaturing gel of in vitro ^{35}S-methionine-labeled transcription/translation reaction products for wild-type and TUBB5 mutants showing similar translational efficiencies.

(L) Kinetic analysis on nondenaturing gels of the products of in vitro transcription/translation reactions for wild-type and TUBB5 mutants. Arrows (top to bottom) denote the migration positions of the chaperonin (CCT)/β-tubulin binary complex (CCT/β), the TBCD/β-tubulin cocomplex, the prefoldin (PFD)/β-tubulin binary complex (PFD/β), the native tubulin heterodimer (α/β), and the TBCA/β-tubulin cocomplex (TBCA/β), each assigned on the basis of their characteristic electrophoretic mobilities. Note that the V353I mutant polypeptide behaved similarly to wild-type controls, whereas there was a diminished heterodimer yield in the case of M299V and little or no detectable heterodimer in the case of E401K. Note also the absence of TBCA/β-tubulin and TBCD/β-tubulin cocomplexes and a relatively long persistence of the PFD/β-tubulin cocomplex in the case of reactions performed with the E401K mutation. Min. chase indicates that reaction products generated after 90 min were further chased with added native bovine brain tubulin so as to drive the generation of tubulin heterodimers for the times shown.

(M–X) Expression of FLAG-tagged wild-type and mutant (M299V, V353I, and E401K) TUBB5 in cultured Neuro-2a cells. Staining with the anti-FLAG antibody is shown in red and the microtubule cytoskeleton visualized using an anti-α-tubulin antibody (shown in green). Note that wild-type FLAG-tagged TUBB5, as well as the corresponding M299V and V353I mutants, incorporated into the microtubule lattice (M–O, P–R, and S–U, respectively). This contrasts with the E401K protein, which is distributed throughout the cytoplasm and failed to incorporate into the cytoskeletal network (V–X). Scale bar in (X) is 10 μm.

See also Figure S3.

real-time PCR followed employing exon spanning primers and three internal control genes. For human studies, fetal brain cDNA was obtained from Yorkshire Biosciences.

In Utero Electroporation Experiments

Sequence-verified constructs for wild-type and mutant versions of *Tubb5* were cloned into pCIG2. shRNAs optimized for specific knockdown of *Tubb5* were cloned into the pSuper vector system. In utero electroporation, cryosectioning, and immunostaining were performed as previously described (Heng et al., 2008; Pacary et al., 2011). Cell counting was performed blind to the condition on representative fields of sections of electroporated brains using ImageJ software.

Biochemical and Cellular Studies

Plasmids encoding the *Tubb5* mutants were expressed in rabbit reticulocyte lysate (Promega) as described (Tian et al., 2010) before analysis on native polyacrylamide gels. For cellular studies, FLAG-tagged TUBB5 DNA constructs were transfected into Neuro-2a cells before immunostaining with an anti-α-tubulin antibody (Sigma, T6199-200UL) and an anti-FLAG antibody (Abcam, ab1162).

Human Studies

We obtained DNA and informed consent according to the guidelines of local institutional review boards at Cochin Hospital and INSERM. *TUBB5* was screened in 120 individuals with sporadic structural brain abnormalities that included lissencephaly, polymicrogyria, microcephaly, and nodular heterotopia. These patients had previously been screened for mutations in the known disease-causing tubulin genes (*TUBA1A, TUBB2B, TUBB3*), and (depending on their phenotype) for other pathogenic genes (e.g., *DCX,*

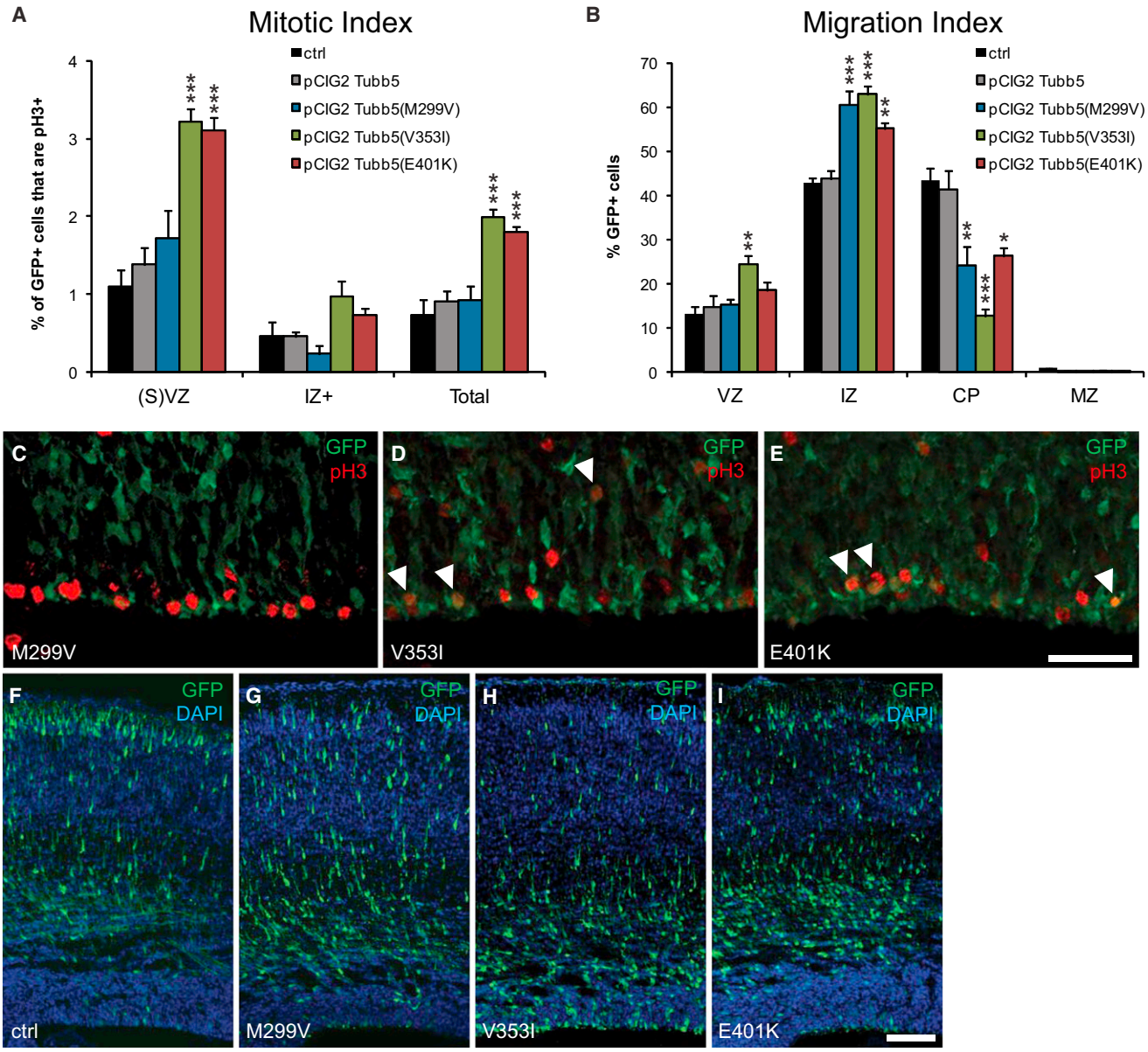

Figure 4. Expression of Disease-Causing *Tubb5* Mutations In Vivo

(A) Quantification of the mitotic index for cells electroporated with control vectors (ctrl), a *Tubb5* expression vector (pCIG2-*Tubb5*; note that this control is also presented in Figure 2B), and the mutants identified (pCIG2-*Tubb5*(M299V), pCIG2-*Tubb5*(V353I), pCIG2-*Tubb5*(E401K)). *Tubb5* overexpression resulted in a mitotic index that was comparable to controls. In contrast, there was a large increase in the percentage of GFP-positive cells that are also pH3 positive in the VZ and SVZ when expressing the E401K and V353I mutant constructs ($n \geq 5$; E401K and V353I: VZ + SVZ: $p < 0.001$; Total: $p < 0.001$). This increase in the mitotic index was also apparent when overexpressing the M299V mutation, although the effect was not statistically significant ($n \geq 5$; $p > 0.05$).

(B) Quantification of the migration index for all five conditions (note that the *Tubb5* overexpression control is also presented in Figure 2G). Overexpression of the mutants results in an accumulation of GFP-positive cells in the IZ with a concomitant decrease in the CP ($n = 5$; M299V: IZ: $p < 0.001$; CP: $p < 0.01$; V353I: VZ: $p < 0.01$; IZ: $p < 0.001$; CP: $p < 0.001$; E401K: IZ: $p < 0.01$; CP: $p < 0.05$) that was not observed when overexpressing *Tubb5* alone ($n = 5$, $p > 0.05$).

(C–E) Representative images used for mitotic index assessment with arrowheads showing colocalization of GFP-expressing cells (green) with pH3 staining (red).

(F–I) Representative images used for migration assessment. Note the decrease in the relative number of cells reaching the upper layers of the cortex when expressing the mutant constructs in comparison to controls (*$p < 0.05$, **$p < 0.01$, ***$p < 0.001$).

Scale bars show 50 μm in (E) and 100 μm in (I). (A) and (B) show mean ± SEM. See also Figure S4.

LIS1, FLNA). Following the identification of de novo mutations in *TUBB5,* parental relationships were confirmed using a suite of microsatellite markers.

Statistics

Statistical analysis was performed with the GraphPad Prism 5 software package. For experiments with two conditions, we performed a Student's

t test. For experiments with multiple conditions, we used a one-way ANOVA followed by Bonferroni multiple comparison test.

For additional details, please see the Extended Experimental Procedures.

SUPPLEMENTAL INFORMATION

Supplemental Information includes Extended Experimental Procedures, four figures, and two tables and can be found with this article online at http://dx.doi.org/10.1016/j.celrep.2012.11.017.

LICENSING INFORMATION

This is an open-access article distributed under the terms of the Creative Commons Attribution-NonCommercial-No Derivative Works License, which permits non-commercial use, distribution, and reproduction in any medium, provided the original author and source are credited.

ACKNOWLEDGMENTS

This study was supported by FWF (P21092, P24367) grants to D.A.K, Fondation pour la Recherche Médicale (Equipe FRM 2007) and ANR (2010 Blanc 1103 01) grants to J.C., and NIH grants (5R01HD057028 and 5R01GM097376) to N.J.C. J.I.H. is supported by an NH and MRC Career Development Fellowship (ID:1011505). The Australian Regenerative Medicine Institute is supported by grants from the State Government of Victoria and the Australian Government. Thanks to Doug Higgs for access to control DNA samples. D.A.K coordinated and designed this study with J.C. and N.J.C. M.B. and A.B. performed the expression studies. J.I.H., M.B., Y.X., M.H., and Z.Q. performed the in vivo murine experiments. D.A.K., T.G., and K.P. performed the genetic screening and sequencing. K.J.H.R., D.S.R., K.T., and M.B. performed the control sequencing. N.B., S.P., M.M., A.V., and P.G. collected and collated the clinical data. T.C. performed the structural modeling. G.T., X.H.J., and N.J.C. undertook the biochemical studies. M.B. conducted the cellular studies with X.H.J. and L.N. M.B. prepared the figures. D.A.K. and M.B. wrote the manuscript, and all authors commented on it.

Received: April 27, 2012
Revised: July 18, 2012
Accepted: November 21, 2012
Published: December 13, 2012

REFERENCES

Ayala, R., Shu, T., and Tsai, L.H. (2007). Trekking across the brain: the journey of neuronal migration. Cell *128*, 29–43.

Braun, A., Breuss, M., Salzer, M.C., Flint, J., Cowan, N.J., and Keays, D.A. (2010). Tuba8 is expressed at low levels in the developing mouse and human brain. Am. J. Hum. Genet. *86*, 819–822, author reply 822–813.

Cowan, N.J., and Lewis, S.A. (2001). Type II chaperonins, prefoldin, and the tubulin-specific chaperones. Adv. Protein Chem. *59*, 73–104.

Edwards, A., Treiber, C.D., Breuss, M., Pidsley, R., Huang, G.J., Cleak, J., Oliver, P.L., Flint, J., and Keays, D.A. (2011). Cytoarchitectural disruption of the superior colliculus and an enlarged acoustic startle response in the Tuba1a mutant mouse. Neuroscience *195*, 191–200.

Feng, Y., and Walsh, C.A. (2001). Protein-protein interactions, cytoskeletal regulation and neuronal migration. Nat. Rev. Neurosci. *2*, 408–416.

Gloster, A., El-Bizri, H., Bamji, S.X., Rogers, D., and Miller, F.D. (1999). Early induction of Talpha1 alpha-tubulin transcription in neurons of the developing nervous system. J. Comp. Neurol. *405*, 45–60.

Heng, J.I., Nguyen, L., Castro, D.S., Zimmer, C., Wildner, H., Armant, O., Skowronska-Krawczyk, D., Bedogni, F., Matter, J.M., Hevner, R., and Guillemot, F. (2008). Neurogenin 2 controls cortical neuron migration through regulation of Rnd2. Nature *455*, 114–118.

Jaglin, X.H., Poirier, K., Saillour, Y., Buhler, E., Tian, G., Bahi-Buisson, N., Fallet-Bianco, C., Phan-Dinh-Tuy, F., Kong, X.P., Bomont, P., et al. (2009). Mutations in the beta-tubulin gene TUBB2B result in asymmetrical polymicrogyria. Nat. Genet. *41*, 746–752.

Keays, D.A., Tian, G., Poirier, K., Huang, G.J., Siebold, C., Cleak, J., Oliver, P.L., Fray, M., Harvey, R.J., Molnár, Z., et al. (2007). Mutations in alpha-tubulin cause abnormal neuronal migration in mice and lissencephaly in humans. Cell *128*, 45–57.

Kim, W.Y., Wang, X., Wu, Y., Doble, B.W., Patel, S., Woodgett, J.R., and Snider, W.D. (2009). GSK-3 is a master regulator of neural progenitor homeostasis. Nat. Neurosci. *12*, 1390–1397.

Kumar, R.A., Pilz, D.T., Babatz, T.D., Cushion, T.D., Harvey, K., Topf, M., Yates, L., Robb, S., Uyanik, G., Mancini, G.M., et al. (2010). TUBA1A mutations cause wide spectrum lissencephaly (smooth brain) and suggest that multiple neuronal migration pathways converge on alpha tubulins. Hum. Mol. Genet. *19*, 2817–2827.

Liu, L., Geisert, E.E., Frankfurter, A., Spano, A.J., Jiang, C.X., Yue, J., Dragatsis, I., and Goldowitz, D. (2007). A transgenic mouse class-III beta tubulin reporter using yellow fluorescent protein. Genesis *45*, 560–569.

Lizarraga, S.B., Margossian, S.P., Harris, M.H., Campagna, D.R., Han, A.P., Blevins, S., Mudbhary, R., Barker, J.E., Walsh, C.A., and Fleming, M.D. (2010). Cdk5rap2 regulates centrosome function and chromosome segregation in neuronal progenitors. Development *137*, 1907–1917.

Löwe, J., Li, H., Downing, K.H., and Nogales, E. (2001). Refined structure of alpha beta-tubulin at 3.5 A resolution. J. Mol. Biol. *313*, 1045–1057.

Neale, B.M., Kou, Y., Liu, L., Ma'ayan, A., Samocha, K.E., Sabo, A., Lin, C.F., Stevens, C., Wang, L.S., Makarov, V., et al. (2012). Patterns and rates of exonic de novo mutations in autism spectrum disorders. Nature *485*, 242–245.

Ohnuma, S., and Harris, W.A. (2003). Neurogenesis and the cell cycle. Neuron *40*, 199–208.

Pacary, E., Heng, J., Azzarelli, R., Riou, P., Castro, D., Lebel-Potter, M., Parras, C., Bell, D.M., Ridley, A.J., Parsons, M., and Guillemot, F. (2011). Proneural transcription factors regulate different steps of cortical neuron migration through Rnd-mediated inhibition of RhoA signaling. Neuron *69*, 1069–1084.

Pinto, D., Pagnamenta, A.T., Klei, L., Anney, R., Merico, D., Regan, R., Conroy, J., Magalhaes, T.R., Correia, C., Abrahams, B.S., et al. (2010). Functional impact of global rare copy number variation in autism spectrum disorders. Nature *466*, 368–372.

Poirier, K., Saillour, Y., Bahi-Buisson, N., Jaglin, X.H., Fallet-Bianco, C., Nabbout, R., Castelnau-Ptakhine, L., Roubertie, A., Attie-Bitach, T., Desguerre, I., et al. (2010). Mutations in the neuronal ß-tubulin subunit TUBB3 result in malformation of cortical development and neuronal migration defects. Hum. Mol. Genet. *19*, 4462–4473.

Tian, G., Jaglin, X.H., Keays, D.A., Francis, F., Chelly, J., and Cowan, N.J. (2010). Disease-associated mutations in TUBA1A result in a spectrum of defects in the tubulin folding and heterodimer assembly pathway. Hum. Mol. Genet. *19*, 3599–3613.

Tischfield, M.A., Baris, H.N., Wu, C., Rudolph, G., Van Maldergem, L., He, W., Chan, W.M., Andrews, C., Demer, J.L., Robertson, R.L., et al. (2010). Human TUBB3 mutations perturb microtubule dynamics, kinesin interactions, and axon guidance. Cell *140*, 74–87.

Tischfield, M.A., Cederquist, G.Y., Gupta, M.L., Jr., and Engle, E.C. (2011). Phenotypic spectrum of the tubulin-related disorders and functional implications of disease-causing mutations. Curr. Opin. Genet. Dev. *21*, 286–294.

Walsh, C.A., and Engle, E.C. (2010). Allelic diversity in human developmental neurogenetics: insights into biology and disease. Neuron *68*, 245–253.